Journal of Materials Chemistry A

Accepted Manuscript

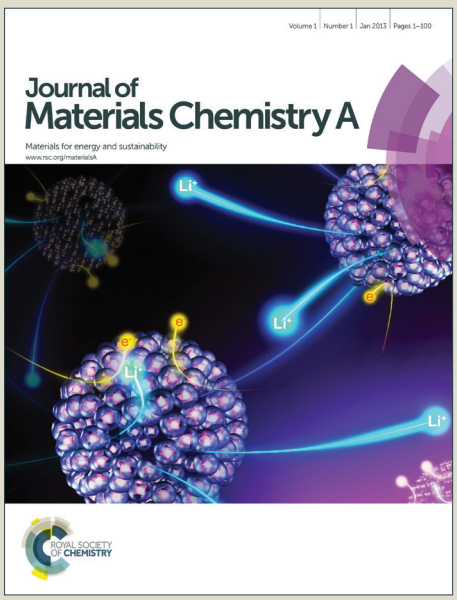

ROYAL SOCIETY OF CHEMISTRY

www.rsc.org/materialsA

Designed Synthesis of Unique Single-crystal Fe-doped $LiNiPO_4$ Nanomesh as the Enhanced Cathode for Lithium Ion Batteries

*Yangyang Feng, Huijuan Zhang, Ling Fang, Ya Ouyang, Yu Wang**

The State Key Laboratory of Mechanical Transmissions and the School of Chemistry and Chemical Engineering, Chongqing University, 174 Shazheng Street, Shapingba District, Chongqing City, P. R. China, 400044;

E-mail: wangy@cqu.edu.cn;

Abstract

In this report, a novel and unique single-crystal hierarchical Fe-doped $LiNiPO_4$ nanomesh is firstly devised and fabricated by a new strategy of super-low crystal mismatch between the precursor and the final sample through *in suit* doping at room temperature. This unique architecture obtained here possesses numerous outstanding properties. Its special two-dimension (2D) morphology can effectively help to shorten pathways for fast lithium ion diffusion and enlarge exposed surface for more lithium-exchange channels. Furthermore, the hierarchical porous structure can be beneficial to the electrolyte's rapid diffusion and Li ions' fast exchange as well as buffer the volume expansion. Importantly, Fe doping into $LiNiPO_4$ can significantly improve the electrical conductivity and the structural stability, so as to enhance Li storage performances. In this work, systematical electrochemical performances of $LiNiPO_4$-based cathode is thoroughly presented for the first time, which is a great breakthrough in high-voltage cathode for LIBs.

Key words: Fe-doped $LiNiPO_4$, single-crystal, hierarchical nanomesh, Li storage.

Introduction

Among the various available electrical energy storage mediums, lithium-ion rechargeable batteries are the most promising power system due to its high energy densities, long cycle life, environmental friendliness and safety.[1, 2] In the last decades, there has been dramatic interest in research and commercial application of lithium ion batteries (LIBs) for large scale energy storage and miniaturization in electronics, especially in portable electronic devices (EV) and plug-in hybrid electric vehicles (PHEV).[3, 4] To our knowledge, there exists the big challenge in electrical-energy storage technology because it cannot be able to keep pace with continuous supply of energy in response to the ever-growing demand, which critically requires high energy density, power rate, safety and low cost.[1, 5-7] For LIBs, it is significant to exploit the enhanced cathode materials for its important impact on battery capacity, stability, safety and cost.[8, 9] Inspired by the success of layered $LiCoO_2$'s commercial developments, researchers have extended their attention on olivine-structured orthophosphates ($LiMPO_4$, where M = Fe, Mn, Co, Ni) owing to their safety, abundant availability, practical discharge capacities as high as ~170 mAh/g and good thermal stability even under vigorous conditions.[10-12] Among the four types of $LiMPO_4$, according to previous computational results, $LiNiPO_4$ possesses the highest operation voltage of 5.1 V vs. Li/Li^+, the highest energy density as well as smaller volume change.[13-15] Additionally, $LiNiPO_4$ has the potential in energy storage not only for superior energy output (> 10.7 Wh) compared to

commercial $LiCoO_2$ (~ 9.9 Wh), but also for lower cost at the same energy production than state-of-the-art cathode.[16, 17]

However, the major drawbacks of sluggish kinetics of the electronic and lithium ion transport for $LiNiPO_4$ cathode exactly restrict the development of $LiNiPO_4$. To circumvent these shortcomings, enlightened by the influence of the crystallinity, morphology and dimensionality on the properties of active functional materials, great efforts on improvement of the intrinsic properties have been made in recent years, including surface cationic doping[18-20], size reduction and conductive substrate coating. Despite the fact that nanoscale materials can enrich active sites and enlarge specific surface area[21, 22], nanocomposites may be easily aggregated and further introduce more structural defects, thereby resulting in rapid decline of specific capacity and poor cycling performance [2, 23]. In other cases, although conductor coating such as carbon or graphene coating can anchor the active material and improve the lifetime of lithium ion batteries,[24] it may bring in low tap density and subsequent reduced energy density.[25] Therefore, enormous applications of sophisticated nanomaterials, particularly with designed and fabricated unique structural details, are always being desperately needed.[26] In recent years, a new strategy, with broadly enlarged specific crystal planes, called crystal engineering, seems a feasible solution to enhance the electrochemical performances due to the fast Li ion transfer.[2, 27-29] As previously reported, two-dimension (2D) membranes with regularly dispersed holes, namely nanosheets, play important roles in energy storage.[23, 30] However, to date, only a few cathode materials with nanomesh morphology have been presented, such as $LiFePO_4$ and $LiCoO_2$, which is initiated by our group.[30] The porous nanomesh possesses many properties. Its unique 2D morphology can effectively help to shorten pathways for fast lithium ion diffusion and enlarge exposed surface for more lithium-exchange channels. Additionally, its porous structure can not only be in favor of the electrolyte's rapid diffusion and Li ions' fast exchange, but also buffer the volume expansion during long-time electrochemical reactions, thereby leading to enhanced electrochemical performances. More importantly, electrode materials with numerous mesoporous can accelerate Li^+ absorption, further to bring higher specific capacity. On the other hand, lattice doping with cations seems to be the most acceptable approach in consider of the fact that doping can strengthen the conductivity, cyclability and improve the specific capacity. As for $LiNiPO_4$, Li^+ mobility is severely limited to 1D tunnels, parallel to [010], specific capacity would be sharply decreased due to the possible immobile Ni^{2+} blocking the channels of Li intercalation/deintercalation.[31, 32] Fe-doping, an alternative strategy for fully charge and discharge, can essentially improve the electrical conductivity and well maintain the structural integrity.[33, 34]

Herein, we introduce a novel single-crystal hierarchical Fe-doped $LiNiPO_4$ ($(Fe)LiNiPO_4$) nanomesh for the first time by a new strategy of super-low crystal mismatch between the precursor and the final sample through *in suit* doping at room temperature. Different from the common porous nanomesh, our hierarchical $(Fe)LiNiPO_4$ nanomesh possesses numerous extraordinary advantages. Its hierarchical porous structure can no doubt enlarge the specific surface area and its special 2D morphology with exposure of specific crystal planes of (010) can exactly reduce the pathways of Li^+ and electron transfer. Importantly, the electrolyte can rapidly percolate and soak through macropores in the primary structure and further intercalate into the mesopores in the second structure, which is beneficial for thorough contact between the electrode materials and electrolyte, thereby resulting in high specific capacity and enhanced rate performance. In addition to the unique hierarchical nanomesh, we are the first to systematically report the electrochemical

performance of $LiNiPO_4$-based cathode. As we know, the general electrolyte could not meet the demand of ultrahigh-voltage $LiNiPO_4$ due to the undesirable decomposition reaction. Moderate Fe-doping can effectively decrease the working voltage of $LiNiPO_4$ in some degree. Significantly, Fe ion can strengthen the structural passability so as to mitigate the capacity attenuation and enhance the cyclic stability. Our novel single-crystal hierarchical (Fe)$LiNiPO_4$ nanomesh exhibits superior rate capability and excellent cyclability, which is absolutely a great breakthrough for $LiNiPO_4$ materials in electrochemical energy storage.

Results and discussion

The whole synthetic process is illustrated in Scheme 1. Similar to our previous work,[35, 36] we use sodium dihydrogen phosphate as phosphorus source and nickel nitrate as nickel source to fabricate uniform $NiNH_4PO_4{\cdot}H_2O$ nanosheets under solvothermal conditions in a large scale. Subsequently, $NiNH_4PO_4{\cdot}H_2O$ nanosheets were immersed in $FeCl_2$ aqueous solution. Due to the near atomic radius, the Fe-doped $NiNH_4PO_4{\cdot}H_2O$ can be prepared through an ion diffusion-exchange process at room temperature. Finally, hierarchical (Fe)$LiNiPO_4$ nanomesh were synthesized by mixed with LiOH powder in a molar ratio of 1:1, followed by high temperature annealing. (Fe)$LiNiPO_4$ crystallizes in an ordered structure with the space group Pnma,[37, 38] which builds up a 3D network with perpendicular tunnels along the (010) and (001) directions, occupied by Li^+ ions.[37, 39] Just as shown in the atomistic model of Fig. S1 (supporting information), the pathway along [010] channel possesses the lowest Li^+ migration energy by calculation, indicating 1 D Li^+ mobility along the b axis during charge and discharge process. This is why researchers try to design crystals with shortened [010] channel. However, Li^+ rapid pathway of [010] may be somewhat restricted by the narrow space among the oxygen anions, which can sharply slow the ionic migrations.[40] In light of this observation, it would be a feasible approach to improve the LIBs performances by increasing mobility of Li^+.

General characterizations of as-prepared $NiNH_4PO_4{\cdot}H_2O$ nanosheets are shown in Fig. 1. As observed in the scanning electron microscopy (SEM) image of Fig. 1a, the sheet-like $NiNH_4PO_4{\cdot}H_2O$ can be easily fabricated in a large scale with the thickness of ~50 nm (shown in inset). The thickness of ~50 nm between 2D and 3D can not only shorten Li^+ diffusion pathway to a certain extent but also reduce structure defects derived from nanoscale materials. The X-ray diffraction (XRD) data in Fig. 1b shows the pure $NiNH_4PO_4{\cdot}H_2O$ with good crystallinity according to the sharpness of peaks from 5 to 90 degrees (JCPDS No.50-0425). Fig. 1c and Fig. 1d are the TEM and HRTEM images of $NiNH_4PO_4H_2O$ nanosheets, respectively. Crystal structure is detected in HRTEM that the crystalline interplanar distance is 0.88 nm for (010) crystal plane. Combining the XRD pattern with the layered structure, it reveals that the prepared $NiNH_4PO_4H_2O$ nanosheets are pure-phase and single crystal. In order to prepare the Fe-doped $NiNH_4PO_4H_2O$, the precursor is mixed with 1 M $FeCl_2$ aqueous solution. Due to the similar atomic size of Fe and Ni, Fe^{2+} can easily exchange with Ni^{2+} through ion diffusion-exchange process. The related characterization of Fe-doped precursor are demonstrated in Fig. S2 and Fig. S3 (supporting information). As revealed in Fig. S2, a small amount of Fe doping hardly effects the sheet-like morphology as well as the crystal structure. From XRD patterns in Fig. S3a, we can observe that the XRD peak position scarcely changes after Fe-doping, but induces a remarkable color change as shown in Fig. S3b.

With the addition of the equivalent molar Li source of LiOH, scalability of single-crystal hierarchical (Fe)$LiNiPO_4$ nanomesh can be feasibly accessible. From the SEM image in Fig. 2a, sheet-like (Fe)$LiNiPO_4$ without any morphological distortion is well inherited by the uniform precursor. In the enlarged SEM image of Fig. 2b, uniform (Fe)$LiNiPO_4$ nanomesh with numerous regular macropores can be clearly detected. The corresponding XRD data is shown in Fig. 2c, in which all the peaks ranging from 10 to 90 degrees match very well with pure $LiNiPO_4$ (JCPDS No.88-1297) and their sharpness uncovers the truth of good crystallinity,[41] further suggesting that Fe impurities introduced in precursor can barely effect the crystal structure of our final samples. By the relevant X-ray energy dispersive spectrum (EDS) analysis in Fig. 2d, it reveals the existence of C, O, Ni, Fe and P, as well as Si derived from the silicon substrate. To better analyze the accurate element content in the final (Fe)$LiNiPO_4$, ICP test is also introduced. The mole ratio of Li, Fe, Ni, P and O is measured as 1.000:0.163:0.838:1.003:4.009, from which we can find that Fe-doping amount is ~16.3% in M2 site. To further clarify the elemental distribution of the final (Fe)$LiNiPO_4$ nanomesh, selected area's elemental imaging of EDS is conducted (Fig. 3). As detected, Ni, Fe, P and O evenly exist in the whole sheet-like samples, confirming Fe doped in the crystal lattice of Ni via ion diffusion-exchange process with low energy consumption at room temperature. This approach may provide a new idea about ion-doping among transition metals. In order to examine the valence states of base elements in final samples, X-ray photoelectron spectroscopy (XPS) is also carried out. The core level photoelectron peaks of Ni 2p, Fe 2p, P 2p and O 1s are shown in Fig. S4 (supporting information). The peak positions are very close to those reported in references,[42-45] indicating the presence of Ni^{2+}, Fe^{2+}, P^{5+} and O^{2-} in as-obtained (Fe)$LiNiPO_4$. These observations further verify Fe doped in M2 site of $LiNiPO_4$ even through a simple ion diffusion-exchange process.

The (Fe)$LiNiPO_4$ nanomesh is further characterized by transmission electron microscopy (TEM). A low-magnification TEM image is presented in Fig. 4a, in which a mesh-like membrane is available. To our knowledge, porous structure can guarantee efficient diffusion pathways for both electrolyte and Li ions, which is beneficial to enhancing the electrochemical performance in long time reactions. Furthermore, the pore space can significantly mitigate the volume change during charge-discharge process to well maintain the structural integrity. Additionally, the sharp crystal lattices are clearly observed and calculated in Fig. 4b. It observes that two inter-perpendicular lattice spacings are 1.01 and 0.47 nm, which separatively corresponds to (100) and (001) plane of (Fe)$LiNiPO_4$. It is indicated that the normal direction is [010] for the (Fe)$LiNiPO_4$ nanomesh through calculation, which is exactly the direction of rapid Li^+ pathway. The regularly extended crystal lattices further confirm that the as-prepared (Fe)$LiNiPO_4$ nanomesh is single crystal. Importantly, the lattice distance of (001) is very close to that of (Fe)$LiNiPO_4$ nanomesh with a near 0% mismatch (Fig. S5, supporting information), which suggests that single crystal (Fe)$LiNiPO_4$ has been successfully fabricated through a tiny crystal mismatch from the precursor.[23, 30] In the magnified TEM image (Fig. 4c), porous structure with dispersed nano-networks can be clearly detected. By carefully examining the architecture of (Fe)$LiNiPO_4$ nanomesh (Fig. 4d), we can find many regularly distributed (Fe)$LiNiPO_4$ nanoparticles and nanoscale void space in the frame of primary structure, thus forming the hierarchical nanomesh. In theory, the hierarchical porous structure can not only inevitably enlarge the specific area of achieved samples, thereby to enhance the contact dimension between electrolyte and active material, but also facilitate electrolyte percolation and soaking. Besides, the presence of void

space can efficiently restrain inner pressure in the electrochemical process, significantly maintaining the structural integrity. To further affirm the hierarchical porous structure our samples possess, N_2 adsorption and desorption isotherms is also introduced, which is an effective measurement to characterize mesoporous materials. As predicted, the specific surface area is ~103.4 m^2/g and the pore size distribution is centered at ~4 nm from Barrete-Joyner-Halenda (BJH) analysis (Fig. 5), consistent with the result from HRTEM image in Fig. 4d. For comparison, BET profile of pure $LiNiPO_4$ nanomesh is also provided (Fig S6. supporting information). The pore distribution of $LiNiPO_4$ ranges from 4-10 nm, further confirms that Fe doping can significantly enhance the uniformity and stability of $LiNiPO_4$-based materials.

To the best of our knowledge, partial substitution of Fe^{2+} into Ni^{2+} can improve the Li^+ mobility in 1 D tunnel crystal structure, along with an enhancement of structural stability. In order to certify the advantages of (Fe)$LiNiPO_4$ compared to $LiNiPO_4$, a series of comparison tests are conducted. We fabricated pure $LiNiPO_4$ nanomesh through the same method expect for Fe doping in the precursor. Fig. S7a (supporting information) is the XRD pattern of pure $LiNiPO_4$ nanomesh, where the baseline is uneven from 10 to 90 degrees. On the contrary, (Fe)$LiNiPO_4$ nanomesh shows a steady baseline with sharp peaks, indicating that Fe doping can significantly enhance the uniformity and crystallinity of $LiNiPO_4$. The corresponding EDS analysis is presented in Fig. S7b (supporting information). Furthermore, the morphology of $LiNiPO_4$ nanomesh is revealed in Fig. S6 (supporting information) for comparison. Fig. S8a and S8c show the (Fe)$LiNiPO_4$ nanomesh in different resolution while Fig. S8b and S8d demonstrate $LiNiPO_4$ nanomesh, from which we can find that the final samples with Fe doping can remarkably strengthen the structural integrity as (Fe)$LiNiPO_4$ nanomesh possesses regular and uniform porous structure. All the observations mentioned above undoubtedly verify that Fe doping can strikingly enhance the crystallinity, uniformity and integrity of $LiNiPO_4$, thus to improve the electrochemical performances for LIBs cathode.

$LiNiPO_4$ is considered as one of the most promising cathode for Li storage. Nevertheless, advances in both ionic and electronic conductivity as well as electrochemical reversibility of $LiNiPO_4$ are rare due to the low conductivity, high operating voltage and some other unknown reasons. Our unique morphology of hierarchical nanomesh may provide a favorable solution to enhance the electrochemical performances of $LiNiPO_4$ to some degree. Herein, a series of electrochemical tests of hierarchical (Fe)$LiNiPO_4$ nanomesh have been investigated. The galvanostatic measurement profiles are described in Fig. 6a. From Fig.6a, we can find a fairly smooth and horizontal voltage plateau of charge, which is little lower than the theoretical value. This observation may be attributed to Fe doping as compared to the pure $LiNiPO_4$ (Fig. S9a, supporting information) and other $LNiPO_4$ cathodes in the literatures.[46] Fe introduced in the lattice of Ni, named solid solutions, can not only properly reduce the working voltage so as to meet the demand of normal electrolyte, but also strengthen the structural passability of $LiNiPO_4$, thereby to enhance the cyclic stability in long time running. Meanwhile, the galvanostatic measurements are performed at a constant rate of 0.1 C over 100 cycles. Noteworthily, our hierarchical (Fe)$LiNiPO_4$ nanomesh exhibits superior reversibility and cyclability compared to pure $LiNiPO_4$ nanomesh (Fig. 6a, supporting information). For the first cycle, the specific capacity is above 180 mAh/g, much higher than the subsequent cycles and even higher than theoretical capacity. This result originates from the irreversible formation of solid electrolyte interface (SEI) resulted from electrolyte degradation, which is pretty common in LIBs cathode. From second cycle, the capacity can reach

up to ~148 mAh/g with a slight decay over 100 cycles, which is a great breakthrough in $LiNiPO_4$-based materials. Cyclic voltammetry (CV) is utilized to trace the oxidation and reduction properties during electrochemical process as shown in Fig. 6b, from which we can see two apparent plateaus at 3 V and 3.7 V. On the contrary, pure $LiNiPO_4$ exhibits no significant oxidation and reduction peaks in CV profile from 2.0-4.95 V (Fig. S9b, supporting information). Generally, it has been reported that $LiNiPO_4$ may present no distinct redox peaks, especially in the potential range of 3.0-5.0 V.[47, 48] The marked plateaus may be derived from Fe doping, in accordance with galvanostatic discharge and charge profile in Fig. 6a. Additionally, there is almost no noticeable changes occur for the CV profiles within 5 cycles, indicating an excellent cyclic stability is available and undoubtedly, a stable and high coulombic efficiency could be provided. In order to uncover the rate capability and enhanced cyclability, consecutive increases in the current density are carried out as revealed in Fig. 6c. The decrease of capacity is unavoidable with the increase of the current densities. With the current density gradually increasing form 0.1 C to 0.2 C, 0.5 C, 1 C, 3 C, the values of specific capacity are changed from 148 mAh/g to 125, 112, 103, 85 mAh/g, respectively. When finally returned to the rate of 0.1 C, the specific capacity can be stabilized at such a high capacity of 129 mAh/g, with a retention of 86.6%. To our knowledge, no capacity as high as 148 mAh/g has been reported for $LiNiPO_4$-based materials. Notably, even though at the ultrahigh rate of 3 C, our unique (Fe)$LiNiPO_4$ nanomesh can reach up to 85 mAh/g, suggesting the architectural advantages of as prepared materials. As a comparison, pure $LiNiPO_4$ nanomesh exhibits a much poor cyclic stability over 30 cycles with a low retention of 36.7% (Fig. S9c, supporting information), indicating Fe doping can exactly improve the cyclic stability and rate performance of $LiNiPO_4$. Fig. 6d is the coulombic efficiency calculated by the ratio of discharge and charge capacities. As expected, the novel hierarchical nanomesh presents excellent stability and coulombic efficiency up to ~88 % over 100 cycles. To highlight the unique structure design, we revisit the status of the (Fe)$LiNiPO_4$ and $LiNiPO_4$ nanomesh. As detected in Fig. S10 (supporting information), the sheet-like nanomesh is perfectly maintained even after a long time running. On the contrary, $LiNiPO_4$ nanomesh exhibits serious aggregation and pulverization during electrochemical reactions (Fig. S11, supporting information), not surprising to reveal a much poor stability. All the above findings verify the fact that the morphological and structural novelty plays a significant role in its functionalization for LIBs cathodes. To affirm the enhanced conductivity of our final samples derived from Fe doping, electrochemical impedance spectrum (EIS) measurement is carried out from 0.01 Hz to 100 Hz. As observed in Fig. S12 (supporting information), our hierarchical (Fe)$LiNiPO_4$ nanomesh exhibits much lower charge transfer impedance than $LiNiPO_4$ nanomesh. To accurately test the conductivity of our samples, the conductivities of both $LiNiPO_4$ and (Fe)$LiNiPO_4$ nanomesh were directly measured by conductance spectra (Table S1, supporting information). It is revealed that conductivities of $LiNiPO_4$ and Fe-doped $LiNiPO_4$ are $3.24*10^{-8}$ and $5.02*10^{-7}$, respectively, further indicating Fe doping could definitely enhance the electronic conductivity and then promote the Li storage performance.

Conclusion

In summary, a novel and unique single-crystal hierarchical (Fe)$LiNiPO_4$ nanomesh has been successfully designed and fabricated through a simple and controllable synthetic method. In this strategy, (Fe)$LiNiPO_4$ nanomesh is achieved via the ion diffusion-exchange process at room

temperature followed by high temperature annealing with addition into Li source. The as-made (Fe)$LiNiPO_4$ nanomesh possesses combined properties of its hierarchical porous structure, single crystallinity and limited thickness. Moreover, it is worth highlighting that Fe doped into M2 site of $LiNiPO_4$ can essentially improve the electrical conductivity and well maintain the structural integrity during long term electrochemical reactions. This advanced architecture as LIBs cathode exhibits high specific capacity (~148 mAh/g), superior cyclic stability and excellent rate performance (no less than 88% capacity retention after 100 cycles), which is absolutely a breakthrough for $LiNiPO_4$ based materials. We believe this work opens up a new gateway for exploiting high-voltage cathode in the next generation of LIBs and undoubtedly this research is of great significance to improve Li storage performances.

Experimental Section

Materials: All chemicals or materials were utilized directly without any further purification before use: ethylene glycol (Fisher Chemical, 99.99%), ammonium hydroxide (NH_3•H_2O, 28–30 wt%, J. T. Baker), nickel nitrate ($Ni(NO_3)_2$, 99.9%, Aldrich), sodium carbonate (Na_2CO_3,99.9%, Aldrich), sodium dihydrogen phosphate(NaH_2PO_4, 99.9%, Aldrich), glucose (Cica-Reagent, Kanto Chemical), ferrous chloride ($FeCl_2$•$4H_2O$, 99.9%, Aldrich) and lithium hydroxide (LiOH, 99.9%, Aldrich).

Preparation of $NiNH_4PO_4$·H_2O nanosheets: In a typical synthesis of $NiNH_4PO_4$·H_2O, concentrated NH_3•H_2O (2.5 mL), ethylene glycol (17.5 mL), 1M $Ni(NO_3)_2$ aqueous solution (1 mL), 1 M NaH_2PO_4 aqueous solution (5mL) and 1 M Na_2CO_3 aqueous solution (1mL) were mixed step-by-step under strong stirring with intervals of 2 min. After that, the precursor solution was stirred for another 5 min, and then the mixture changed into bluish green solution. Afterwards, the precursor solution was transferred into a Teflon-lined stainless-steel autoclave with a volume of 50 mL. And thermal treatment was performed on the Teflon liner in an electric oven at 170 ^oC for 24 h. After the autoclave was cooled naturally to room temperature in air, samples deposited at the bottom of Teflon were collected and washed by centrifugation for at least three cycles by using deionized water and one cycle by using pure ethanol. The as-synthesized samples were then dried in a normal oven at 60 ^oC overnight to remove the absorbed water and ethanol for the subsequent fabrication and characterizations.

Preparation of Fe-doped $NiNH_4PO_4$•H_2O nanosheets: The as-prepared $NiNH_4PO_4$•H_2O nanosheets (250 mg) were ultrasonically mixed with 40 mL $FeCl_2$ aqueous solution (1 M) to form a homogeneous solution. The mixture was standing for 2 h at room temperature until the color of the nanosheets slowly turned to yellow-green. Finally, the samples were washed for three cycles by deionized water and one cycle by ethanol, and then dried in a normal oven at 60 ^oC.

Preparation of hierachical (Fe)$LiNiPO_4$ **nanomesh:** Fe-doped $NiNH_4PO_4$•H_2O nanosheets were mixed with stoichiometric molar ratio of LiOH. Subsequently, the (Fe)$LiNiPO_4$ nanomesh was synthesized by calcinations in the tube furnace under Ar atmosphere at 650 ^oC for 200 min with a ramp of 1 ^oC/min.

Characterization of the samples: A field-emission scanning electron microscope (SEM) coupled with an EDX analyzer (JEOL, JSM-7800F, 2 kV, 15 kV), TEM coupled with an EDX analyzer (Philips, Tecnai, F30, 300 kV), powder X-ray diffraction with Cu Kα radiation (XRD, Bruker D8 Advance), BET surface-area measurement of surface-area and pore-size analyzer (Quantachrome Autosorb-6B) and X-ray photoelectron spectrometery with a ESCA-LAB250 analyzer (XPS) were employed to characterize the obtained samples, inductively coupled plasma-atomic emission spectroscopy (ICP-AES, iCAP 6300Duo).

Electrochemical testing: For electrochemical tests, the working electrodes were prepared by a slurry coating procedure. The slurry which consisted of 80 wt.% (Fe)$LiNiPO_4$ nanomesh, 10 wt.% carbon black and 10 wt.% polyvinylidene fluoride (PVDF) dissolved in a few drops of N-methyl pyrrolidinone (NMP), was incorporated under magnetic stirring for at least 1 days to form a homogeneous mixture. Then the compound was spread on Al foils with 12 mm diameter. The mass loading of the electrode material is 0.8-1.2 mg/cm^2. After dried at 90^oC for 24 h in vacuum, the samples were assembled in an argon-filled glove box under a pressure of 20 Mpa. The obtain pieces of nickel foam covered with samples were used as working electrodes, the metallic lithium foil (99.9%, Aldrich) as the counter electrodes, 1 M $LiPF_6$ in ethylene carbonate (EC)/dimethyl

carbonate (DME) (1: 1 in volume) as the electrolyte, and a polypropylene (PP) microporous film (Cellgard2400) as the separator. The galvanostatic charge–discharge tests were conducted on a NEWARE battery program-control test system at rates of 0.1-3 C (1 C=168 mA/g) in the voltage range of 2.0–4.95 V at room temperature (25 ^{o}C). Cyclic voltammetry (CV) and electrochemical impedance spectrum (EIS) were performed on CH660E electrochemical work station. CV measurements were recorded between 2 and 4.95 V (versus Li/Li^{+}) at a scan rate of 0.5 mV/s.

Acknowledgements

This work was financially supported by the Thousand Young Talents Program of the Chinese Central Government (Grant No.0220002102003), National Natural Science Foundation of China (NSFC, Grant No. 21373280，21403019), Beijing National Laboratory for Molecular Sciences (BNLMS), the Fundamental Research Funds for the Central Universities (0301005202017) and Hundred Talents Program at Chongqing University (Grant No. 0903005203205).

Supporting Information Available: More SEM, TEM, EDS, XRD, XPS and electrochemical testing data are available in the supporting information for this paper.

References

1. M. Armand and J. M. Tarascon, *Nature*, 2008, **451**, 652-657.
2. P. G. Bruce, B. Scrosati and J.-M. Tarascon, *Angew. Chem. Int. Ed.*, 2008, **47**, 2930-2946.
3. O. K. Park, Y. Cho, S. Lee, H.-C. Yoo, H.-K. Song and J. Cho, *Energ Environ Sci.*, 2011, **4**, 1621-1633.
4. G. Jeong, Y.-U. Kim, H. Kim, Y.-J. Kim and H.-J. Sohn, *Energ Environ Sci.*, 2011, **4**, 1986-2002.
5. C.-C. Hu, K.-H. Chang, M.-C. Lin and Y.-T. Wu, *Nano Lett.*, 2006, **6**, 2690-2695.
6. V. Etacheri, R. Marom, R. Elazari, G. Salitra and D. Aurbach, *Energ Environ Sci.*, 2011, **4**, 3243-3262.
7. J. J. Wang and X. L. Sun, *Energ Environ Sci.*, 2012, **5**, 5163-5185.
8. J. Yang, J. Wang, Y. Tang, D. Wang, X. Li, Y. Hu, R. Li, G. Liang, T.-K. Sham and X. Sun, *Energ Environ Sci.*, 2013, **6**, 1521-1528.
9. X. Zhi, G. Liang, L. Wang, X. Ou, J. Zhang and J. Cui, *J. Power Sources*, 2009, **189**, 779-782.
10. A. K. Padhi, K. S. Nanjundaswamy and J. B. Goodenough, *J. Electrochem. Soc.*, 1997, **144**, 1188-1194.
11. K. Amine, H. Yasuda and M. Yamachi, *Electrochem. Solid-State Lett.*, 2000, **3**, 178-179.
12. A. V. Murugan, T. Muraliganth, P. J. Ferreira and A. Manthiram, *Inorg. Chem.*, 2009, **48**, 946-952.
13. Q. D. Truong, M. K. Devaraju and I. Honma, *J. Mater. Chem. A*, 2014, **2**, 17400-17407.
14. F. Zhou, C. A. Marianetti, M. Cococcioni, D. Morgan and G. Ceder, *Phys. ReV. B*, 2004, **69**, 201101.
15. F. Zhou, M. Cococcioni, K. Kang and G. Ceder, *Electrochem. Commn.*, 2004, **6**, 1144-1148.
16. S. M. Rommel, N. Schall, C. Brunig and R. Weihrich, *Monatsh.Chem.*, 2014, **145**, 385-404.
17. W. F. Howard and R. M. Spotnitz, *J. Power Sources*, 2007, **165**, 887-891.
18. L. Dimesso, D. Becker, C. Spanheimer and W. Jaegermann, *J.Solid State Electrochem.*, 2012, **16**, 3791-3798.
19. L. Dimesso, C. Spanheimer and W. Jaegermann, *Mater. Res.Bull.*, 2013, **48**, 559-565.
20. R. Qing, M.-C. Yang, Y. S. Meng and W. Sigmund, *Electrochim. Acta*, 2013, **108**, 827-832.
21. Y. Li, H. Wang, L. Xie, Y. Liang, G. Hong and H. Dai, *J. Am. Chem. Soc.*, 2011, **133**, 7296-7299.
22. H. Zhang, Y. Feng, Y. Zhang, L. Fang, W. Li, Q. Liu, K. Wu and Y. Wang, *Chemsuschem*, 2014, **7**, 2000-2006.
23. Y. Wang, H. J. Zhang, J. Wei, C. C. Wong, J. Y. Lin and A. Borgna, *Energ Environ Sci.*, 2011, **4**, 1845-1854.
24. J. L. Yang, L. Hu, J. X. Zheng, D. P. He, L. L. Tian, S. C. Mu and F. Pan, *J Mater Chem A*, 2015, **3**, 9601-9608.
25. K. Saravanan, P. Balaya, M. V. Reddy, B. V. R. Chowdari and J. J. Vittal, *Energ Environ Sci.*, 2010, **3**, 457-463.
26. H. J. Zhang, Y. Y. Feng, Y. Zhang, L. Fang, W. X. Li, Q. Liu, K. Wu and Y. Wang,

Chemsuschem, 2014, **7**, 2000-2006.

27. H. J. Zhang, Y. J. Bai, Y. Zhang, X. Li, Y. Y. Feng, Q. Liu, K. Wu and Y. Wang, *Sci. Rep.*, 2013, **3**.
28. L. Wang, X. M. He, W. T. Sun, J. L. Wang, Y. D. Li and S. S. Fan, *Nano Lett.*, 2012, **12**, 5632-5636.
29. X. Rui, X. Zhao, Z. Lu, H. Tan, D. Sim, H. H. Hng, R. Yazami, T. M. Lim and Q. Yan, *ACS Nano*, 2013, **7**, 5637-5646.
30. H. J. Zhang, C. C. Wong and Y. Wang, *Cryst. Growth Des.*, 2012, **12**, 5629-5634.
31. H. Fang, Z. Pan, L. Li, Y. Yang, G. Yan, G. Li and S. Wei, *Electrochem. Commn.*, 2008, **10**, 1071-1073.
32. D. Morgan, A. Van der Ven and G. Ceder, *Electrochem. Solid-State Lett.*, 2004, **7**, A30-A32.
33. F. C. Strobridge, D. S. Middlemiss, A. J. Pell, M. Leskes, R. J. Clement, F. Pourpoint, Z. G. Lu, J. V. Hanna, G. Pintacuda, L. Emsley, A. Samoson and C. P. Grey, *J. Mater. Chem. A*, 2014, **2**, 11948-11957.
34. J. Wolfenstine and J. Allen, *J Power Sources*, 2004, **136**, 150-153.
35. Y. Y. Feng, Y. OuYang, L. Peng, H. J. Qiu, H. L. Wang and Y. Wang, *J Mater Chem A*, 2015, **3**, 9587-9594.
36. Y. Feng, H. Zhang, Y. Mu, W. Li, J. Sun, K. Wu and Y. Wang, *Chemistry – A European Journal*, 2015, **21**, 9229-9235.
37. C. M. Julien, A. Mauger, K. Zaghib, R. Veillette and H. Groult, *Ionics*, 2012, **18**, 625-633.
38. C. V. Ramana, A. Ait-Salah, S. Utsunomiya, U. Becker, A. Mauger, F. Gendron and C. M. Julien, *Chem. Mater.*, 2006, **18**, 3788-3794.
39. S. Geller and J. L. Durand, *Acta. Cryst.*, 1960, **13**, 325-331.
40. B. L. Ellis, K. T. Lee and L. F. Nazar, *Chem. Mater.*, 2010, **22**, 691-714.
41. E. Muthuswamy, G. H. L. Savithra and S. L. Brock, *ACS Nano*, 2011, **5**, 2402-2411.
42. P. Y. Shih, S. W. Yung and T. S. Chin, *J. Non-Cryst. Solids*, 1998, **224**, 143-152.
43. Y. J. Park, Y. S. Hong, X. L. Wu, K. S. Ryu and S. H. Chang, *J Power Sources*, 2004, **129**, 288-295.
44. Q. Li, G. S. Li, C. C. Fu, D. Luo, J. M. Fan and L. P. Li, *Acs Appl. Mater. Inter.*, 2014, **6**, 10330-10341.
45. K. S. Park, A. Benayad, M. S. Park, A. Yamada and S. G. Doo, *Chem. Commun.*, 2010, **46**, 2572-2574.
46. J. Wolfenstine and J. Allen, *J. Power Sources*, 2004, **136**, 150-153.
47. S. Okada, S. Sawa, M. Egashira, J.-i. Yamaki, M. Tabuchi, H. Kageyama, T. Konishi and A. Yoshino, *J. Power Sources*, 2001, **97–98**, 430-432.
48. J. Wolfenstine and J. Allen, *J. Power Sources*, 2005, **142**, 389-390.

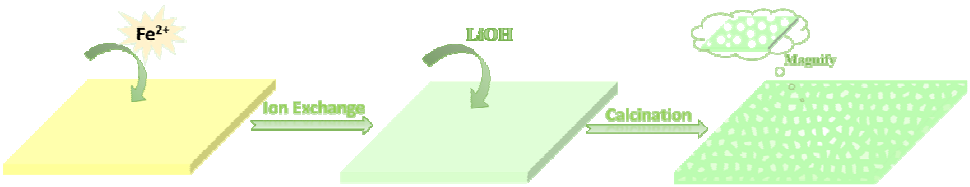

Scheme 1. Schematic illustration of the fabrication route from the precursor of $NiNH_4PO_4•H_2O$ nanosheets to Fe-doped $NiNH_4PO_4•H_2O$ nanosheets and finally to the hierarchical (Fe)$LiNiPO_4$ nanomesh.

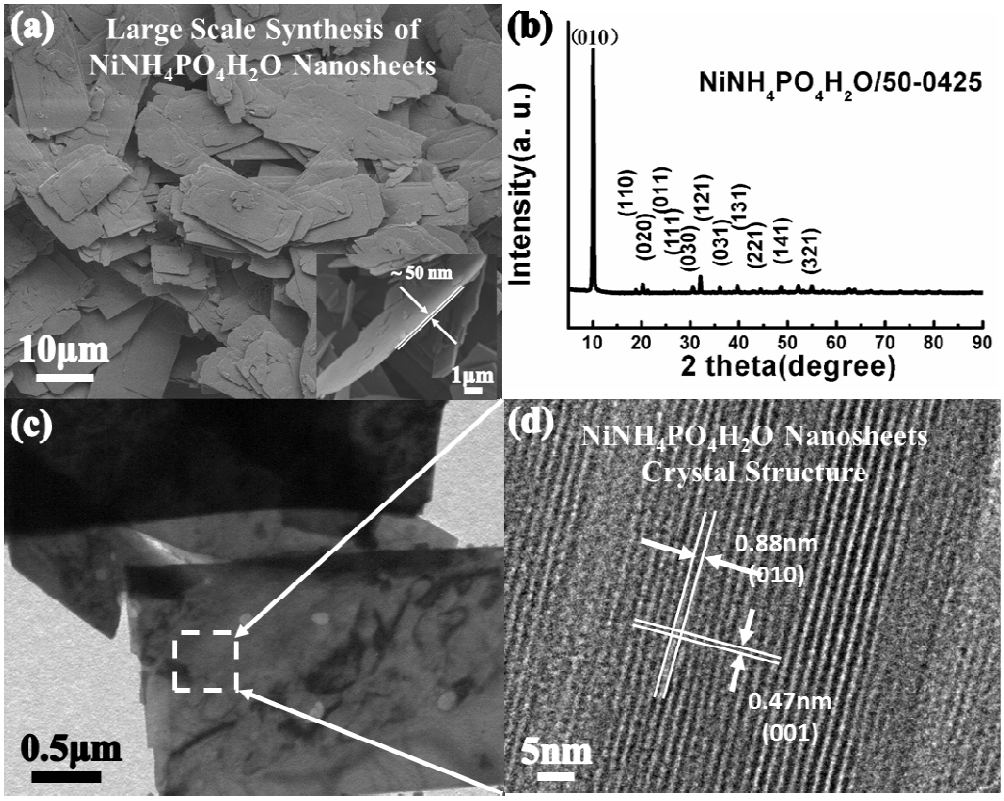

Figure 1. Typical characterizations of $NiNH_4PO_4 \cdot H_2O$ nanosheets. (a) Low-magnification SEM image to clarify the uniformity and scalability of $NiNH_4PO_4 \cdot H_2O$ nanosheets. (b) XRD data to verify the pure-phase of $NiNH_4PO_4 \cdot H_2O$ nanosheets. (c) TEM image and (d) HRTEM image of synthesized $NiNH_4PO_4 \cdot H_2O$ nanosheets to clearly demonstrate sheet-like morphology and the crystal structure.

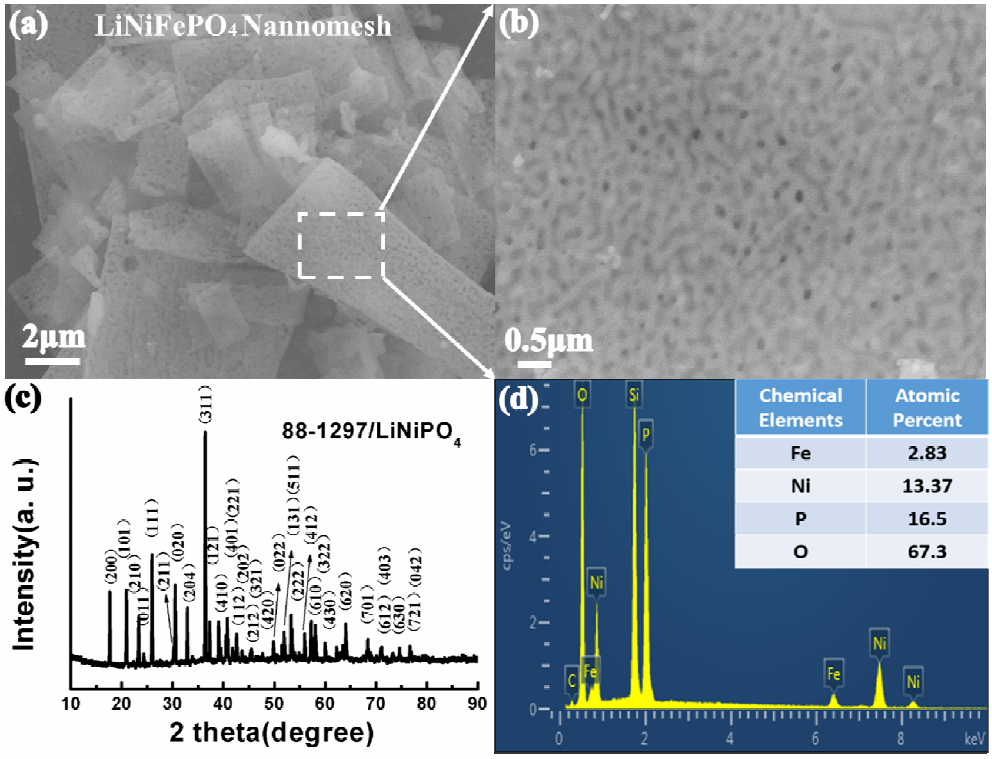

Figure 2. SEM images at lower (a) and higher (b) resolutions to demonstrate (Fe)$LiNiPO_4$ nanomesh. (c) XRD pattern form 10 to 90 degrees at 2 theta to show the pure-phase of (Fe)$LiNiPO_4$. (d) The corresponding EDS analysis to verify the existence of Fe, Ni, P and O.

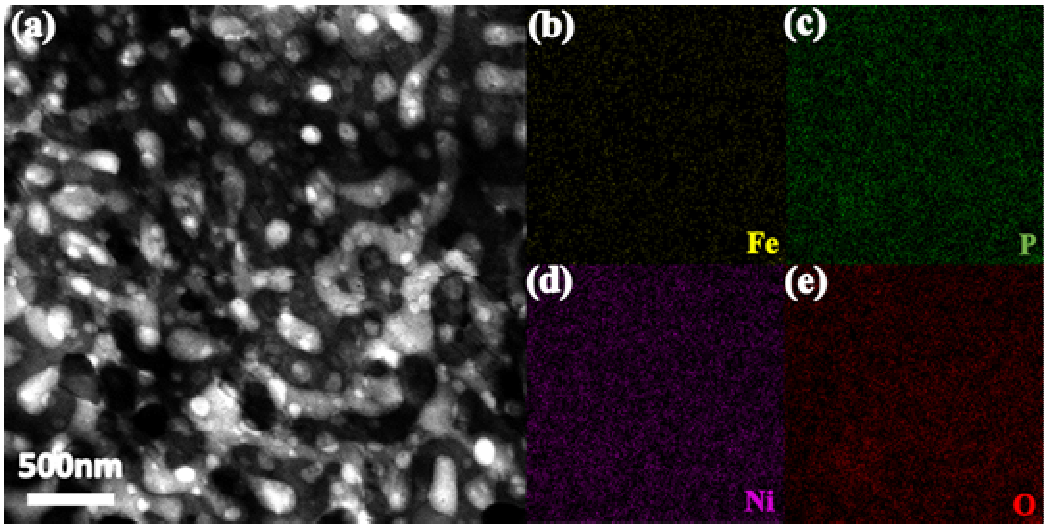

Figure 3. Elemental images via EDX shows the element distribution of the (Fe)$LiNiPO_4$. (a) The TEM image. The presence and distribution of Fe, P, Ni and O are demonstrated in (b), (c), (d) and (e) respectively.

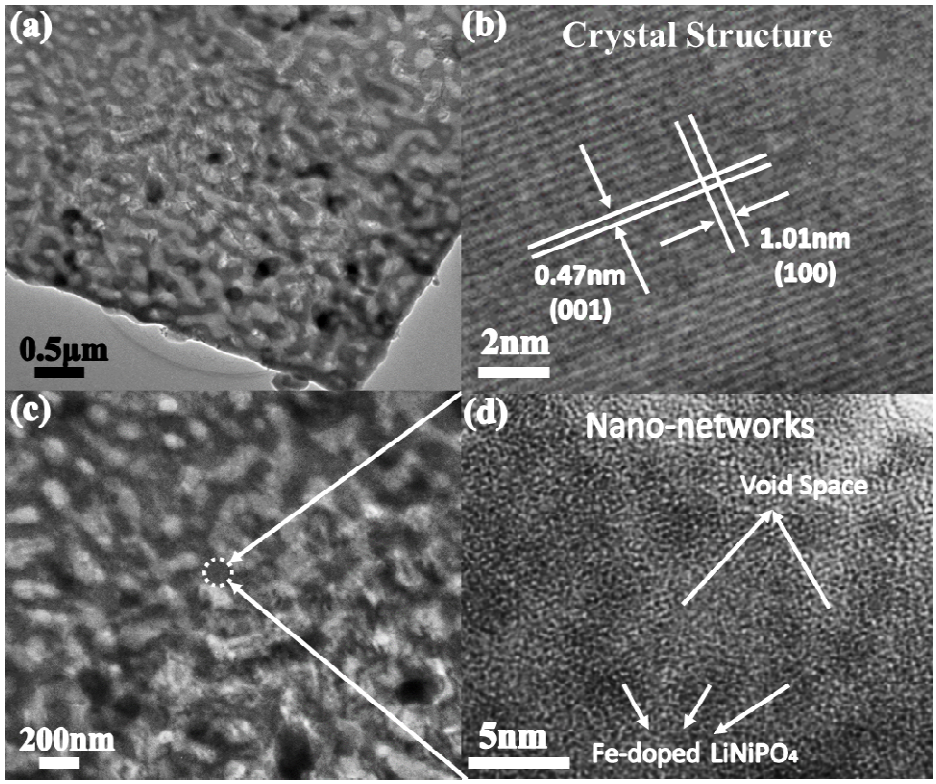

Figure 4. (a) Low-magnification TEM and (b) HRTEM images of (Fe)$LiNiPO_4$. (c) the magnified TEM image and (d) partial enlarged HRTEM image of (Fe)$LiNiPO_4$, in which many regular nanoparticles and void space are clearly detected, confirming that we fabricated hierarchical (Fe)$LiNiPO_4$ nanomesh.

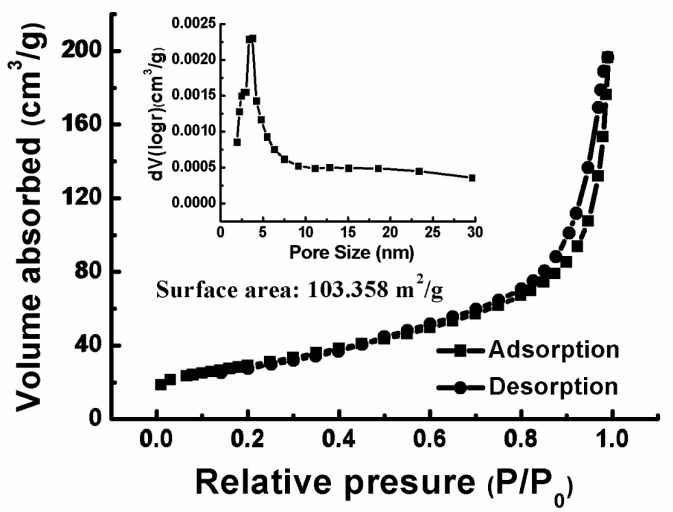

Figure 5. BET profile of the hierarchical (Fe)$LiNiPO_4$ nanomesh to present the specific surface area and the pore size distribution derived from the desorption branch (inset).

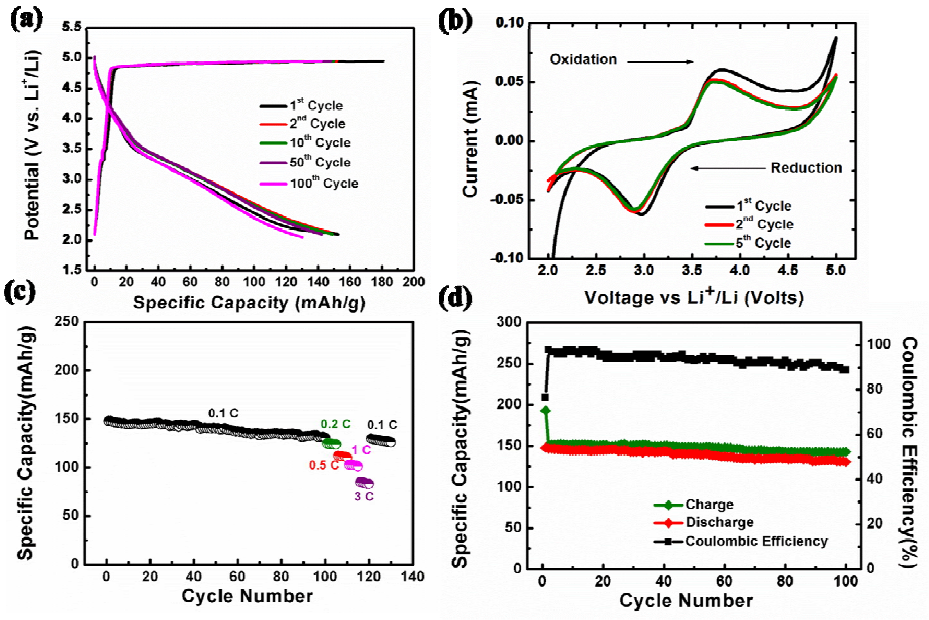

Figure 6. Electrochemical measurements are applied to characterize (Fe)$LiNiPO_4$ nanomesh. (a) galvanostatic measurements over 100 charge/discharge cycles. (b) Cyclic voltammetry (CV) profiles. (c) Rate capability performance at various current densities from 0.1 C to 3 C. (d) the evaluation of coulombic efficiency at 0.1 C.

Table of Contents:

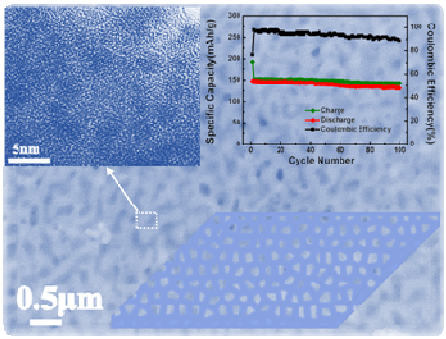

We report a novel and unique single-crystal hierarchical Fe-doped $LiNiPO_4$ nanomesh and its systematical electrochemical performances for LIBs, which is a great breakthrough in $LiNiPO_4$-based materials.